Establishing metrics to quantify underlying structure in vascular red blood cell distributions

Sayan Roychowdhury[1], Erik W. Draeger[2], and Amanda Randles[1]

[1] Dept of Biomedical Engineering, Duke University, Durham NC 27705, USA
sayan.roychowdhury@duke.edu
amanda.randles@duke.edu
[2] Center for Applied Scientific Computing,
Lawrence Livermore National Laboratory, Livermore CA, USA
draeger1@llnl.gov

Abstract. Simulations of the microvasculature can elucidate the effects of various blood flow parameters on micro-scale cellular and fluid phenomena. At this scale, the non-Newtonian behavior of blood requires the use of explicit cell models, which are necessary for capturing the full dynamics of cell motion and interactions. Over the last few decades, fluid-structure interaction models have emerged as a method to accurately capture the behavior of deformable cells in the blood. However, as computational power increases and systems with millions of red blood cells can be simulated, it is important to note that varying spatial distributions of cells may affect simulation outcomes. Since a single simulation may not represent the ensemble behavior, many different configurations may need to be sampled to adequately assess the entire collection of potential cell arrangements. In order to determine both the number of distributions needed and which ones to run, we must first establish methods to identify well-generated, randomly-placed cell distributions and to quantify distinct cell configurations. In this work, we utilize metrics to assess 1) the presence of any underlying structure to the initial cell distribution and 2) similarity between cell configurations. We propose the use of the radial distribution function to identify long-range structure in a cell configuration and apply it to a randomly-distributed and structured set of red blood cells. To quantify spatial similarity between two configurations, we make use of the Jaccard index, and characterize sets of red blood cell and sphere initializations.

Keywords: red blood cells · microvascular simulation · cell packing

1 Introduction

Computational blood flow models are a powerful tool for answering biomedical questions. For microvessel simulations, where individual cell diameters are on the same order of magnitude as vessel size, the presence of cells plays a significant role in the non-Newtonian behavior of blood. In this regime, velocity profile blunting has been observed due to the motion of cells towards the vessel centerline[1] and blood viscosity has been shown to be dependent on vessel diameter

ICCS Camera Ready Version 2022
To cite this paper please use the final published version:
DOI: 10.1007/978-3-031-08751-6_7

and hematocrit (volume percentage of cells in the blood)[2]. Additionally, cell-to-cell[3] and cell-to-vessel interactions[4] have been shown to affect the underlying blood flow profile. Therefore in small vessel simulations, blood must be modeled as a suspension of cells rather than a continuum fluid. Fluid-structure interaction (FSI) models, such as the immersed boundary method[5] or dissipative particle dynamics[6], which fully couple deformable particles with a background fluid, have been shown to accurately model cells in microfluidic[7] and microcirculatory systems[8]. Blood flow simulations using FSI models provide a wealth of information, as both microscopic and macroscopic quantities, such as individual cell position and deformation, and fluid pressure and velocity profiles, can be precisely tracked and studied over time[9, 10]. More importantly, these models allow for the isolation and controlled variation of specific parameters such as cell size or stiffness, enabling researchers to probe the effects of individual parameters on the quantity of interest. Much of the *in silico* work in microvessels with cell FSI models has been focused on red blood cells (RBCs), including studies on the effects of cell deformability and shape[11–13], partitioning at junctions in the vasculature[14, 15], aggregation mechanics[16], and development of a cell-depleted layer[17, 18]. Simulation has also been used to study the motion of other particles in the presence of RBCs such as platelets[19, 20], leukocytes[21, 22], and circulating tumor cells[23–25, 10, 26].

While FSI models of cells in complex geometries are not new, advances in computational efficiency and capability[27–30] have only recently made this approach practical for comprehensive studies of realistic systems. The inclusion of explicit particles in particular introduces several new obstacles. The main challenge is simply one of statistics: the motion of particles diffusing through a vessel is an inherently stochastic process, thus trajectories must be sampled a sufficient number of times to capture average behavior. For example, when tracking cancer cells *in silico*, the distance to a vessel wall directly influences the cell's likelihood of adhesion[31] and subsequent escape into nearby tissue. We previously demonstrated the effects of varying cell positions while studying combinations of hemodynamic parameters and the motion of a tumor cell[23]. Even when all bulk fluid parameters were held constant, the trajectory of the tumor cell was found to vary significantly based on the relative configurations of neighboring cells.

In addition to increasing the overall computational cost, the need for a representative ensemble of starting configurations introduces new potential sources of error that must be managed. This challenge is particularly acute for systems with higher hematocrit values, where random coordinate generation must be done carefully to avoid artificial structure that would bias the observed dynamics. Similar to the well-known equilibration problem in molecular dynamics[32], flow simulations through tortuous vascular geometries have the added complication that one can not easily gather equilibrated statistics simply by running a closed system longer in time. Instead, one must generate a number of distinct sets of equilibrated starting points to be run independently[33]. To this end, we propose a method to generate many cell configurations and the use of the radial

ICCS Camera Ready Version 2022
To cite this paper please use the final published version:
DOI: 10.1007/978-3-031-08751-6_7

distribution function to characterize the structure in a particular configuration. The final challenge is to define quantitative metrics to rigorously compare individual cell configurations and to characterize the complete set as a whole. For this purpose, we propose the use of the Jaccard index to quantify spatial similarity between individual configurations as an appropriate metric for describing and comparing sets of cell configurations.

2 Methods and Metrics

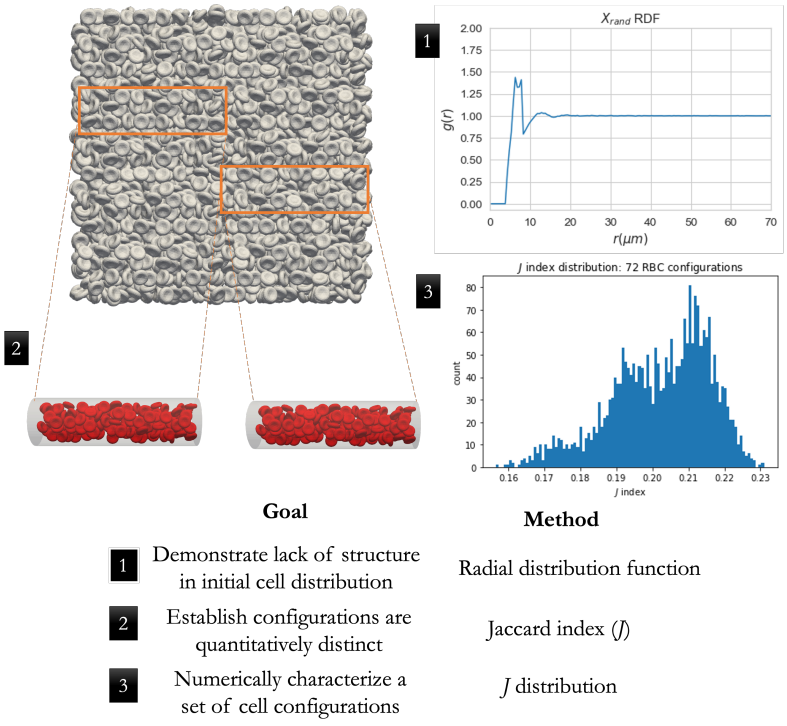

Fig. 1. Workflow for determining the best set of cell configurations to describe the ensemble. (1) The radial distribution function $g(r)$ is used to assess randomness in a distribution of cells. (2) The Jaccard index J is used to quantify spatial similarity between two configurations. (3) A set of pairwise J values are used to numerically describe a large set of cell configurations and presented as a distribution.

Our proposed workflow and associated metrics are shown in Figure 1. In this section, we will describe both the methods we use to generate cell configurations as well as the associated metrics used to characterize them.

ICCS Camera Ready Version 2022
To cite this paper please use the final published version:
DOI: 10.1007/978-3-031-08751-6_7

2.1 Generating initial configurations of red blood cells in a microvessel

Dense packing of non-overlapping shapes is a long-standing research problem of active interest[34–36]. Here we describe a procedure for generating and characterizing packed configurations of RBCs in arbitrary vessels at a set hematocrit. Rather than generating individual configurations on demand, we instead start with a large system of packed cells from which we can fill vessels of arbitrary size and shape. This technique has the advantage of letting us generate a packed domain in the simplest possible geometry prior to simulation while avoiding the code complexity an on-the-fly implementation would require. The source domain is created to be several times larger than the vessel of interest. The standalone implementation provided by Birgin *et al.*[37] is used to pack ellipsoids that tightly encompass the RBC's biconcave shape, returning a set of non-overlapping positions and orientations. Although the fully enclosed RBC represents approximately 70% of the encompassing ellipsoid volume, a distribution with a packing fraction of up to 60% is enough to reach the high end of microvascular hematocrit levels. An example of this packing and a corresponding cell initialization is shown in Figure 2. Testing vessels ranging in diameter from 20 to 50 µm shows the ability to reach realistic hematocrits from 20% to 35% consistently.

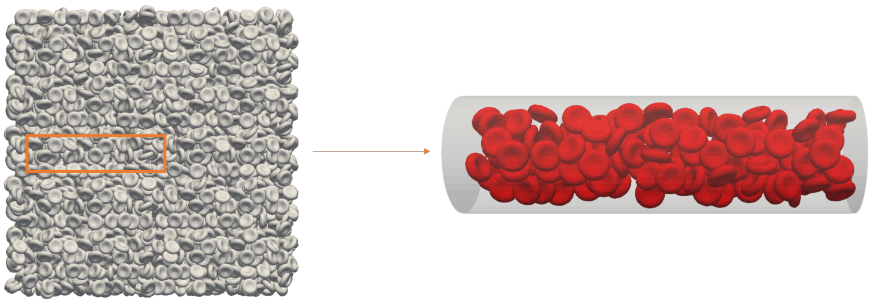

Fig. 2. An example of a cell initialization taken by submerging the vessel within a large, pre-generated packing domain. Only cells that fit completely inside the vessel are returned and used as the starting point for a simulation.

This approach of separately generating a packed source domain has the advantage of easily allowing for rigorous *a priori* analysis before performing expensive high performance computing (HPC) simulations. To avoid initializing FSI runs with non-physical starting configurations, the source bulk system must not have any long-range order consistent with crystalline packing. The radial distribution function $g(r)$ is a well-established metric in the simulation of fluids[38] used for confirming liquid structure, defined as:

ICCS Camera Ready Version 2022
To cite this paper please use the final published version:
DOI: 10.1007/978-3-031-08751-6_7

$$g(r) = \frac{dn_c}{4\pi r^2 dr\rho} \tag{1}$$

where dn_c returns the number of cells within a shell of thickness dr and ρ is the bulk density. Long-range structure is reflected in the form of multiple peaks well beyond the average particle spacing. RBCs are assumed to start from a fully disordered liquid state, reflected by a $g(r)$ that quickly converges to a constant value of unity.

Once the bulk source geometry has been generated, individual configurations can be created by submerging the target vessel in the source domain at different locations and selecting all cells contained within. This process remains the same for both simple and complex geometries, establishing a straightforward method for generating many different configurations prior to running HPC simulations.

2.2 Quantifying spatial similarity between cell configurations

After generating a set of multiple cell configurations, the next step is to verify that each of these packings are distinct by quantifying their spatial similarity to each other; specifically, the fraction of volume shared by two configurations. However, due to the irregular biconcave disk shape of RBCs, a simple analytical algorithm for overlap check given cell positions and orientation angles does not exist. Therefore in this calculation, a numerical method is utilized, where each configuration of RBCs is mapped to a 3-D grid, and overlap is calculated by the number of grid points shared. The Jaccard index, or intersection over union, is used to measure the similarity between two discrete sample sets, defined as:

$$J(C_i, C_j) = \frac{|C_i \cap C_j|}{|C_i \cup C_j|} \tag{2}$$

where C_i and C_j are independent samples of the same space. We propose the use of the Jaccard index to quantify the volume overlap between sets of RBCS by comparing the interior grid points. This is similar in approach to the algorithms used by the image segmentation community[39], such as the Dice similarity index.

Since $J(C_i, C_j)$ represents the percentage of overlapping cell volume between C_i and C_j, $J(C_i, C_j) = 100\%$ if two arrangements are identical and zero if there is no shared cell volume in space. A threshold value ϕ is chosen to label whether or not two configurations are correlated; if $J(C_i, C_j) > \phi$, the pair is marked similar. For example, two test configurations that contained the same group of cells shifted by a few tenths of a microns led to J over 90%, and would be marked as a similar pair. Because the likelihood of two configurations of cells both occupying a certain space increases with hematocrit, ϕ is not a static value, and is chosen on a per hematocrit basis.

A two-dimensional example for calculating J using RBCs is provided in Figure 3. Each initialization contains a single cell marked red for configuration 1 and blue for configuration 2. The corresponding lattice points are marked with the

ICCS Camera Ready Version 2022
To cite this paper please use the final published version:
DOI: 10.1007/978-3-031-08751-6_7

color of containing cell. Once these two lattices are overlaid, the shared points are marked in yellow.

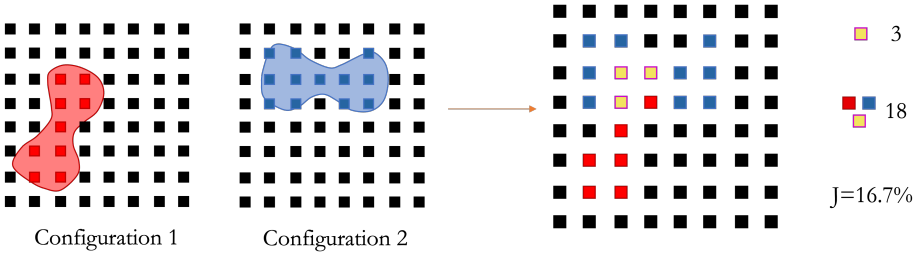

Fig. 3. A 2-D example for the calculation of Jaccard index J between two configurations of RBCs. After the RBCs are mapped to their corresponding lattices, there are 18 total points which contain a cell, of which 3 are shared in both configurations. $J = 3/18 = 16.7\%$ in this example.

Another two-dimensional visual example is shown in Figure 4, displaying distinct configurations of circles with significantly different J values. Compared to the base configuration, there is a clear difference in overlap, which can be identified visually and captured quantitatively through an analytical computation of J.

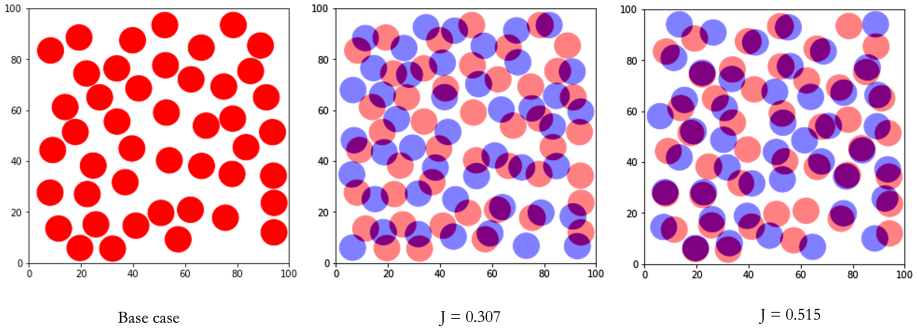

Fig. 4. A 2-D example of differing Jaccard indices compared to a base configuration (left) using circular particles. Two other distinct configurations are generated and overlaid on the base configuration (middle and right). The middle configuration is less similar to the base case than the right configuration and can be confirmed visually by identifying by the overlapping violet regions and computed using J. Although the overlap is easier to visualize in 2-D, it is much easier to numerically identify similarity in 3-D space by using J.

ICCS Camera Ready Version 2022
To cite this paper please use the final published version:
DOI: 10.1007/978-3-031-08751-6_7

Although these examples are displayed in two dimensions for clarity, our RBC configurations and future simulations are performed in three-dimensional space. The Jaccard index provides a numerical method to identify spatial similarity rather than a qualitative comparison.

Since the Jaccard index is applied between two particular configurations, J needs to be calculated on a pairwise basis before it can be used to quantify the entire distribution of configurations. For a set of configurations $S = \{C_1, ..., C_n\}$, we define J_S, the set of Jaccard similarity scores, as:

$$J_S = \{J(C_i, C_j) \big| i, j = 1...n, i \neq j\}. \tag{3}$$

To quantify the similarity of a particular configuration C_i with respect to all the others, the mean Jaccard index $\bar{J}(C_i)$ is calculated as:

$$\bar{J}(C_i) = \frac{1}{n-1} \sum_{j=1}^{n} J(C_i, C_j), j \neq i \tag{4}$$

for a set of n configurations. Given two similar configurations C and C' such that $J(C, C') > \phi$, and mean Jaccard indices such that $\bar{J}(C) < \bar{J}(C')$, configuration C' would be considered first for removal from the set.

3 Results and Discussion

3.1 Applying the radial distribution function to quantify structure in a single packing

To test for the presence of long-range structure, the radial distribution function $g(r)$ is applied to two large, dense packings of RBCs. Both source arrangements are generated in a cubic domain of side length 200 µm with over 35,000 cells. A random distribution X_{rand} is created by packing the cube and then applying an external force to perturb the initial arrangement of cells, while a structured set of cells X_{struct} is produced by tessellating a small set of RBCs across the space. The radial distribution function is then applied to each set of cell centers splitting dr into 0.25 µm buckets, and the cell configurations and corresponding $g(r)$ functions are shown in Figure 5.

Within X_{rand}, $g(r)$ contains a single peak near the lengthwise diameter of the RBC that quickly trails off to unity, indicative of a liquid-like, random distribution of particles. In the case of X_{struct}, multiple discrete peaks are visible, signifying the presence of long-range structure in the distribution of cells. A qualitative comparison between the two source domains can be performed visually, but the use of the radial distribution functions provide a quantitative confirmation for the presence of ordered structure.

Since the procedure to generate many cell configurations in a microvessel utilizes a subset of the cells in the large domain, it is important to confirm the randomness of the initial cell arrangements. The packing found in X_{struct} is non-physiological, and would generate many structured cell initializations as inputs

ICCS Camera Ready Version 2022
To cite this paper please use the final published version:
DOI: 10.1007/978-3-031-08751-6_7

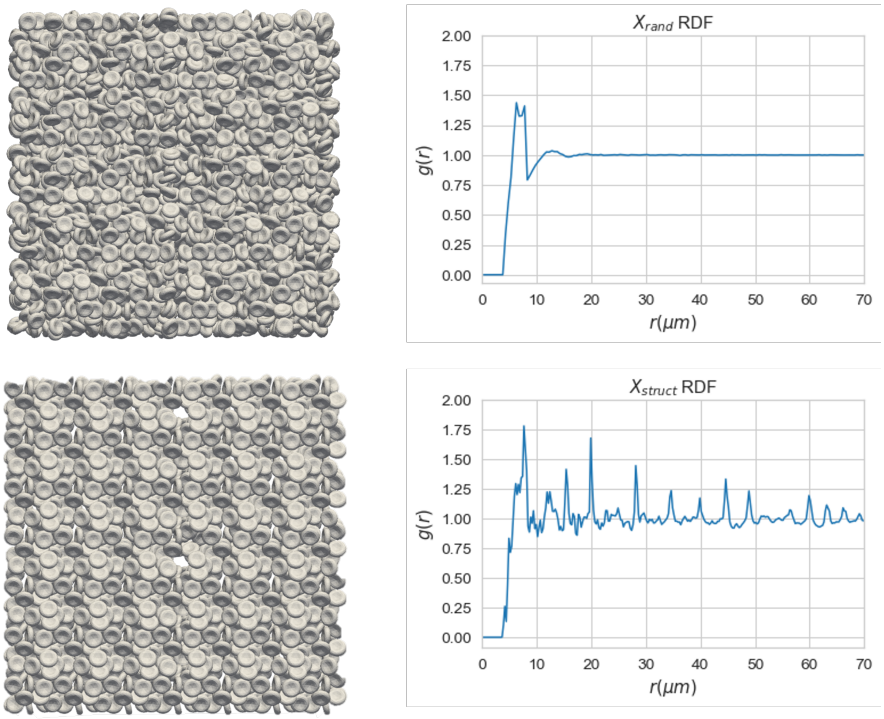

Fig. 5. A random distribution X_{rand} (top) and ordered distribution X_{struct} (bottom) of cells packed within a cube of side length 200 µm. The corresponding radial distribution functions are shown to the right. X_{rand}'s $g(r)$ shows a single peak and trails off to 1 quickly, analogous to a random liquid-like state, while X_{struct}'s $g(r)$ displays several peaks, indicating that the distribution contains a repetitive structure. Sampling cells from the random distribution provides a better initial set of the positions and orientations of red blood cells for running HPC simulations.

ICCS Camera Ready Version 2022
To cite this paper please use the final published version:
DOI: 10.1007/978-3-031-08751-6_7

to HPC simulations. Moving forward, we sample configurations from X_{rand} after confirming the lack of long-range structure in its distribution of cells.

3.2 Utilizing Jaccard index to quantify distributions of cell configurations

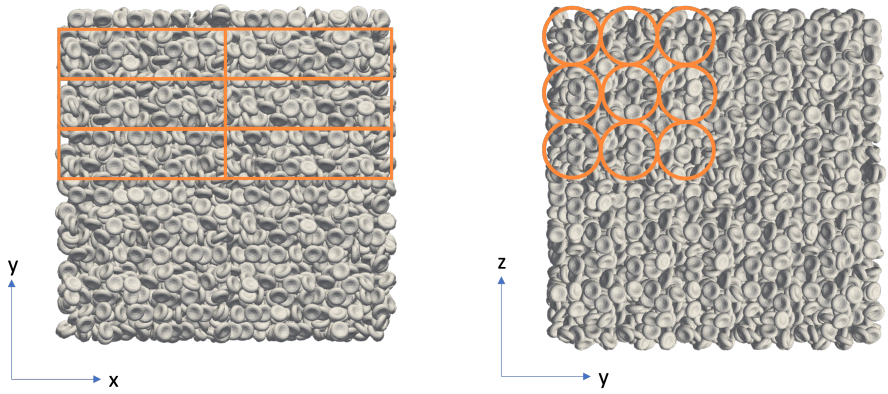

Fig. 6. There are 72 different non-overlapping initializations for a cylinder of diameter 30 µm and length 100 µm pulled from a packing domain of 200^3 µm^3. Cells within this region are used to generate RBC configurations of initial positions and orientations at a target hematocrit of 25%. A subset of the cutouts are shown in each xy and yz planes for this set of initializations.

Non-overlapping cutouts representing an ideal microvessel geometry with diameter 30 µm and length 100 µm are created from X_{rand}. The dimensions of the source geometry allow for 72 independent configurations to be generated: 6 from the y- and z-planes, and 2 in the x-plane, as shown in Figure 6. All configurations have a hematocrit of 25% with $N = 160$ RBCs on average. The Jaccard index is calculated using a grid spacing of 0.25 µm. A histogram of all pairwise Jaccard similarity index values is presented in Figure 7a. For comparison, random configurations of 160 spheres were numerically generated at a 25% packing density in a cylinder with the same aspect ratio (see Figure 7b-d). We note that increasing the number of configurations for better statistics gave smoother distributions but did not fundamentally change the shape.

As expected, the overlap index of configurations of randomly-placed spheres follows a normal distribution. The distribution of RBCs, on the other hand, is clearly skewed away from normal. This may be an artifact of the packing algorithm used to populate the source distribution X_{rand} or may be a fundamental difference in how biconcave disks pack into a confined geometry; more work will

ICCS Camera Ready Version 2022
To cite this paper please use the final published version:
DOI: 10.1007/978-3-031-08751-6_7

be needed to elucidate the underlying cause. The magnitude of the average overlap differs significantly between the shapes as well despite all systems having the same volume packing fraction. It should be noted that the RBC geometry likely has a systematic underestimation of the overlap due to discretization error, though this is not expected to be large. The spherical overlap was computed analytically as a function of distance between sphere centers. Figure 8 shows $\bar{J}$, the average pair overlap of a configuration with all other configurations. This provides a method to compare individual configurations' spatial coverage against the full set. We expect that both J_S and $\bar{J}$ distributions will change based on vessel geometry and hematocrit. However, this study establishes that a pairwise Jaccard index distribution can be used as a quantitative metric to describe a set of cell configurations, generated with the same packing fraction. We posit that selecting configurations with low $\bar{J}$ could be used to sample the configurational phase space more efficiently; this will be the topic of a follow-up study.

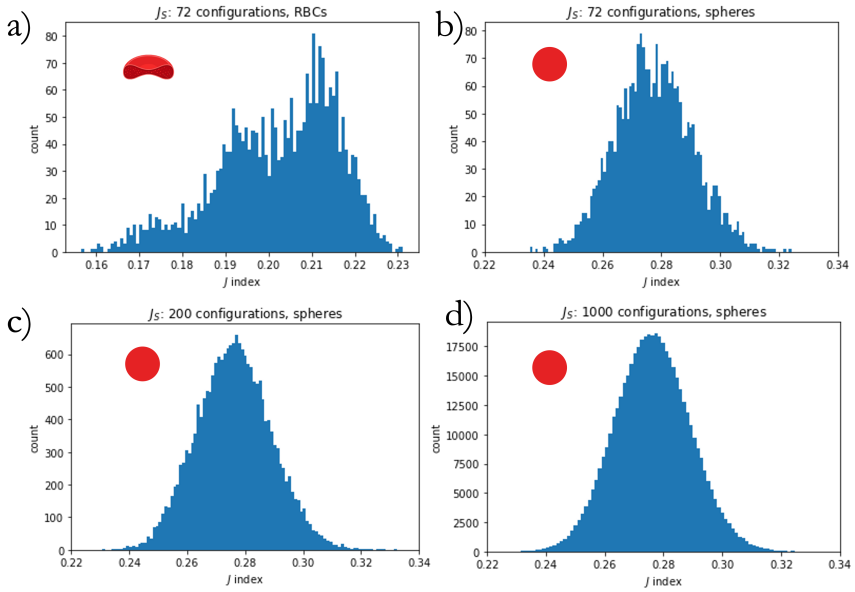

Fig. 7. The distribution J_S of pairwise J values for (a) RBC and (b-d) sphere configurations. N=160 objects.

4 Conclusion

In the microvessel regime, FSI models are used to perform simulations with explicit RBCs to account for non-Newtonian effects. Now that recent computational advances have enabled the rise of large-scale FSI simulation studies, it is

ICCS Camera Ready Version 2022
To cite this paper please use the final published version:
DOI: 10.1007/978-3-031-08751-6_7

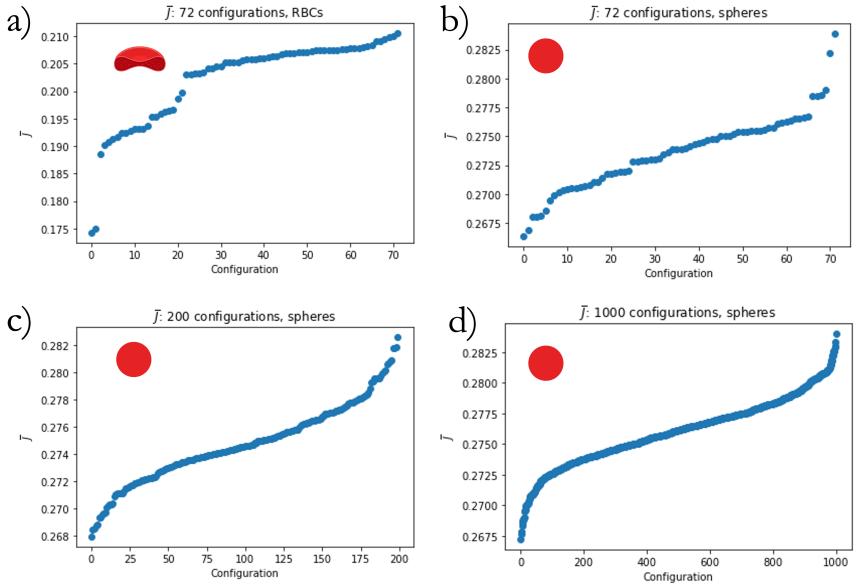

Fig. 8. Distribution of $\bar{J}$ on a per configuration basis for (a) RBC and (b-d) sphere configurations. N=160 objects.

important to sufficiently sample the ensemble of potential cell arrangements to capture a macroscopic behavior. In order to select the minimum set of configurations that spans the parameter space, certain quantitative metrics must be established which (1) indicate that a particular configuration is a good starting point and (2) show that two separate arrangements are distinct and spatially uncorrelated. These parameters can then be used to define the space of possible configurations and determine which set of arrangements best span the space.

In this study, we apply the radial distribution function to particular configurations of RBCs to qualify whether a structured arrangement of cells exists in the distribution. We choose two large distributions of cells, one randomly placed and one structured, analogous to atoms in liquid- and solid-like materials, and show that this function is able to quantify the presence of long-range structure in cell positions. We also use the Jaccard index J to capture a quantitative representation of shared cell volume between two configurations. Taking the irregular shape of RBCs into account, we devise a numerical method that maps cells on to a 3-D lattice which is used to compute J. We then produce a set of 72 RBC configurations in a 30 µm diameter and 100 µm length microvessel from the randomly-distributed group of RBCs. For comparison, we also generate sets of 72, 200, and 1000 configurations of spheres at the same packing fraction. Finally, we perform pairwise J calculations and plot the distribution of Jaccard index values, showing that this metric can be used to define the space of particle configurations.

ICCS Camera Ready Version 2022
To cite this paper please use the final published version:
DOI: 10.1007/978-3-031-08751-6_7

This study sets the groundwork for identifying the optimal set of initial cell arrangements for a specific group of simulation parameters. Next steps for this work include performing simulation studies with sets of spatially uncorrelated RBC configurations to determine how these affect certain outputs, such as motion of individual cells. Future work will also study the effect of different vessel sizes, shapes, and hematocrit on distributions of the Jaccard similarity index.

5 Acknowledgments

The authors would like to thank Daniel Puleri and Samreen Mahmud for their feedback and discussion. This work was performed under the auspices of the U.S. Department of Energy by Lawrence Livermore National Laboratory under Contract DE-AC52-07NA27344. Computing support for this work came from the Lawrence Livermore National Laboratory (LLNL) Institutional Computing Grand Challenge program. The work of Sayan Roychowdhury and Amanda Randles was supported by the National Science Foundation under award number 1943036. The content is solely the responsibility of the authors and does not necessarily represent the official views of the NSF.

References

1. Tangelder, G.J., Slaaf, D.W., Muijtjens, A., Arts, T., Oude Egbrink, M., Reneman, R.S.: Velocity profiles of blood platelets and red blood cells flowing in arterioles of the rabbit mesentery. Circulation Research **59**(5), 505–514 (1986)
2. Pries, A.R., Neuhaus, D., Gaehtgens, P.: Blood viscosity in tube flow: dependence on diameter and hematocrit. American Journal of Physiology-Heart and Circulatory Physiology **263**(6), H1770–H1778 (1992)
3. Bishop, J.J., Nance, P.R., Popel, A.S., Intaglietta, M., Johnson, P.C.: Effect of erythrocyte aggregation on velocity profiles in venules. American Journal of Physiology-Heart and Circulatory Physiology **280**(1), H222–H236 (2001)
4. Panés, J., Perry, M., Granger, D.N.: Leukocyte-endothelial cell adhesion: avenues for therapeutic intervention. British journal of pharmacology **126**(3), 537 (1999)
5. Peskin, C.S.: The immersed boundary method. Acta numerica **11**, 479–517 (2002)
6. Pivkin, I.V., Karniadakis, G.E.: Accurate coarse-grained modeling of red blood cells. Physical review letters **101**(11), 118105 (2008)
7. Krüger, T., Holmes, D., Coveney, P.V.: Deformability-based red blood cell separation in deterministic lateral displacement devices—a simulation study. Biomicrofluidics **8**(5), 054114 (2014)
8. Fedosov, D.A., Noguchi, H., Gompper, G.: Multiscale modeling of blood flow: from single cells to blood rheology. Biomechanics and modeling in mechanobiology **13**(2), 239–258 (2014)
9. Bagchi, P.: Mesoscale simulation of blood flow in small vessels. Biophysical journal **92**(6), 1858–1877 (2007)
10. Pepona, M., Balogh, P., Puleri, D.F., Hynes, W.F., Robertson, C., Dubbin, K., Alvarado, J., Moya, M.L., Randles, A.: Investigating the interaction between circulating tumor cells and local hydrodynamics via experiment and simulations. Cellular and Molecular Bioengineering **13**(5), 527–540 (2020)

ICCS Camera Ready Version 2022
To cite this paper please use the final published version:
DOI: 10.1007/978-3-031-08751-6_7

11. Lei, H., Karniadakis, G.E.: Quantifying the rheological and hemodynamic characteristics of sickle cell anemia. Biophysical journal **102**(2), 185–194 (2012)
12. Czaja, B., Gutierrez, M., Závodszky, G., de Kanter, D., Hoekstra, A., Eniola-Adefeso, O.: The influence of red blood cell deformability on hematocrit profiles and platelet margination. PLoS Computational Biology **16**(3), e1007716 (2020)
13. Krüger, T., Holmes, D., Coveney, P.V.: Deformability-based red blood cell separation in deterministic lateral displacement devices—a simulation study. Biomicrofluidics **8**(5), 054114 (2014)
14. Balogh, P., Bagchi, P.: Analysis of red blood cell partitioning at bifurcations in simulated microvascular networks. Physics of Fluids **30**(5), 051902 (2018)
15. Yang, J., Yoo, S.S., Lee, T.R.: Effect of fractional blood flow on plasma skimming in the microvasculature. Physical Review E **95**(4), 040401 (2017)
16. Zhang, J., Johnson, P.C., Popel, A.S.: Red blood cell aggregation and dissociation in shear flows simulated by lattice boltzmann method. Journal of biomechanics **41**(1), 47–55 (2008)
17. Fedosov, D.A., Caswell, B., Popel, A.S., Karniadakis, G.E.: Blood flow and cell-free layer in microvessels. Microcirculation **17**(8), 615–628 (2010)
18. Katanov, D., Gompper, G., Fedosov, D.A.: Microvascular blood flow resistance: role of red blood cell migration and dispersion. Microvascular research **99**, 57–66 (2015)
19. Vahidkhah, K., Diamond, S.L., Bagchi, P.: Platelet dynamics in three-dimensional simulation of whole blood. Biophysical journal **106**(11), 2529–2540 (2014)
20. Fitzgibbon, S., Spann, A.P., Qi, Q.M., Shaqfeh, E.S.: In vitro measurement of particle margination in the microchannel flow: effect of varying hematocrit. Biophysical journal **108**(10), 2601–2608 (2015)
21. Jain, A., Munn, L.L.: Determinants of leukocyte margination in rectangular microchannels. PloS one **4**(9), e7104 (2009)
22. Freund, J.B.: Leukocyte margination in a model microvessel. Physics of Fluids **19**(2), 023301 (2007)
23. Roychowdhury, S., Gounley, J., Randles, A.: Evaluating the influence of hemorheological parameters on circulating tumor cell trajectory and simulation time. In: Proceedings of the Platform for Advanced Scientific Computing Conference. pp. 1–10 (2020)
24. Xiao, L., Lin, C., Chen, S., Liu, Y., Fu, B., Yan, W.: Effects of red blood cell aggregation on the blood flow in a symmetrical stenosed microvessel. Biomechanics and modeling in mechanobiology **19**(1), 159–171 (2020)
25. Gounley, J., Draeger, E.W., Randles, A.: Numerical simulation of a compound capsule in a constricted microchannel. Procedia computer science **108**, 175–184 (2017)
26. Balogh, P., Gounley, J., Roychowdhury, S., Randles, A.: A data-driven approach to modeling cancer cell mechanics during microcirculatory transport. Scientific reports **11**(1), 1–18 (2021)
27. Grinberg, L., Insley, J.A., Morozov, V., Papka, M.E., Karniadakis, G.E., Fedosov, D., Kumaran, K.: A new computational paradigm in multiscale simulations: Application to brain blood flow. In: Proceedings of 2011 International Conference for High Performance Computing, Networking, Storage and Analysis. pp. 1–5 (2011)
28. Ames, J., Puleri, D.F., Balogh, P., Gounley, J., Draeger, E.W., Randles, A.: Multi-gpu immersed boundary method hemodynamics simulations. Journal of computational science **44**, 101–153 (2020)

ICCS Camera Ready Version 2022
To cite this paper please use the final published version:
DOI: 10.1007/978-3-031-08751-6_7

29. Lu, L., Morse, M.J., Rahimian, A., Stadler, G., Zorin, D.: Scalable simulation of realistic volume fraction red blood cell flows through vascular networks. In: Proceedings of the International Conference for High Performance Computing, Networking, Storage and Analysis. pp. 1–30 (2019)
30. Gounley, J., Draeger, E.W., Randles, A.: Immersed boundary method halo exchange in a hemodynamics application. In: International Conference on Computational Science. pp. 441–455. Springer (2019)
31. Xiao, L., Liu, Y., Chen, S., Fu, B.: Effects of flowing rbcs on adhesion of a circulating tumor cell in microvessels. Biomechanics and modeling in mechanobiology **16**(2), 597–610 (2017)
32. Stella, L., Melchionna, S.: Equilibration and sampling in molecular dynamics simulations of biomolecules. The Journal of chemical physics **109**(23), 10115–10117 (1998)
33. Gordiz, K., Singh, D.J., Henry, A.: Ensemble averaging vs. time averaging in molecular dynamics simulations of thermal conductivity. Journal of Applied Physics **117**(4), 045104 (2015)
34. Donev, A., Cisse, I., Sachs, D., Variano, E.A., Stillinger, F.H., Connelly, R., Torquato, S., Chaikin, P.M.: Improving the density of jammed disordered packings using ellipsoids. Science **303**(5660), 990–993 (2004)
35. Malmir, H., Sahimi, M., Tabar, M.: Microstructural characterization of random packings of cubic particles. Scientific reports **6**(1), 1–9 (2016)
36. Miśkiewicz, K., Banasiak, R., Niedostatkiewicz, M., Grudzień, K., Babout, L.: An algorithm to generate high dense packing of particles with various shapes. In: MATEC Web of Conferences. vol. 219, p. 05004. EDP Sciences (2018)
37. Birgin, E.G., Lobato, R.D.: A matheuristic approach with nonlinear subproblems for large-scale packing of ellipsoids. European Journal of Operational Research **272**(2), 447–464 (2019)
38. Allen, M.P., Tildesley, D.J.: Computer simulation of liquids. Oxford university press (2017)
39. Yeghiazaryan, V., Voiculescu, I.D.: Family of boundary overlap metrics for the evaluation of medical image segmentation. Journal of Medical Imaging **5**(1), 015006 (2018)

ICCS Camera Ready Version 2022
To cite this paper please use the final published version:
DOI: 10.1007/978-3-031-08751-6_7